Published in final edited form as:
Bioorg Med Chem Lett. 2014 September 15; 24(18): 4466–4471. doi:10.1016/j.bmcl.2014.07.091.

Facile synthesis of SSR180575 and discovery of 7-chloro-*N,N*,5-trimethyl-4-oxo-3(6-[^{18}F]fluoropyridin-2-yl)-3,5-dihydro-4*H*-pyridazino[4,5-*b*]indole-1-acetamide, a potent pyridazinoindole ligand for PET imaging of TSPO in cancer

Yiu-Yin Cheung[a], **Michael L. Nickels**[a,b], **Dewei Tang**[a,b], **Jason R. Buck**[a,b], and **H. Charles Manning**[a,b,c,d,e,f]

[a]Vanderbilt University Institute of Imaging Science (VUIIS), Vanderbilt University Medical Center, Nashville, Tennessee 37232

[b]Department of Radiology and Radiological Sciences, Vanderbilt University Medical Center, Nashville, Tennessee 37232

[c]Program in Chemical and Physical Biology, Vanderbilt University Medical Center, Nashville, Tennessee 37232

[d]Vanderbilt-Ingram Cancer Center (VICC), Vanderbilt University Medical Center, Nashville, Tennessee 37232

[e]Department of Biomedical Engineering, Vanderbilt University, Nashville, Tennessee 37232

[f]Department of Neurosurgery, Vanderbilt University Medical Center, Nashville, Tennessee 37232

Abstract

A novel synthesis of the translocator protein (TSPO) ligand 7-chloro-*N*,*N*,5-trimethyl-4-oxo-3-phenyl-3,5-dihydro-4*H*-pyridazino[4,5-*b*]indole-1-acetamide (SSR180575, **3**) was achieved in four steps from commercially available starting materials. Focused structure−activity relationship development about the pyridazinoindole ring at the N3 position led to the discovery of 7-chloro-*N*,*N*,5-trimethyl-4-oxo-3(6-fluoropyridin-2-yl)-3,5-dihydro-4*H*-pyridazino[4,5-*b*]indole-1-acetamide (**14**), a novel ligand of comparable affinity. Radiolabeling with fluorine-18 (^{18}F) yielded 7-chloro-*N*,*N*,5-trimethyl-4-oxo-3(6-[^{18}F]fluoropyridin-2-yl)-3,5-dihydro-4*H*-pyridazino[4,5-*b*]indole-1-acetamide (^{18}F-**14**) in high radiochemical yield and specific activity. *In vivo* studies of [^{18}F]-**14** revealed this agent as a promising probe for molecular imaging of glioma.

Correspondence to: H. Charles Manning.

Supplementary Material

Synthetic and analytical results for all compounds; methods; supplemental figures. This material is available free of charge *via* the Internet at:

Keywords

TSPO; Glioma; PET; Fluorine-18; SSR180575

There exists a continuing demand for the development and validation of improved imaging biomarkers for cancer. Such biomarkers may aid in cancer diagnosis, predict clinical outcome, and quantify response to therapeutic intervention. Imaging biomarkers of glioma are limited and routinely include magnetic resonance imaging (MRI), computed tomography (CT), and less frequently, positron emission tomography (PET). Of these, PET may be the most suitable given its exquisite sensitivity, quantitative nature, and ability to analyze the molecular basis of the tumor. For most oncology studies, 2-deoxy-2-[^{18}F]fluoroglucose ([^{18}F]FDG) is commonly utilized, as this tracer reflects glucose metabolism, which is usually elevated in cancer cells.[1] However, relatively high glucose uptake in normal brain results in poor tumor-to-background ratios that can confound glioma detection. Moreover, [^{18}F]FDG uptake can be affected by a myriad of tangential metabolic processes. This has led many groups to evaluate other PET tracers of metabolism in this setting, including amino acid–based PET probes such as [^{11}C]MET,[2] [^{18}F]FET,[3] and [^{18}F]FDOPA.[4] While these probes can accumulate in tissues that exhibit enhanced amino acid transport,[5-7] they can be hampered by nonspecific accumulation.[6] Thus, there remains a need to develop and validate additional PET imaging biomarkers suitable for glioma detection and characterization.

We have explored translocator protein (TSPO) expression as a target for molecular imaging of cancer with PET.[8-13] TSPO, formerly the peripheral benzodiazepine receptor (PBR), is an 18 kDa protein that takes part in a wide breadth of cellular processes, including cell proliferation, apoptosis, steroid biosynthesis, and cholesterol metabolism.[14] Though TSPO has historically been leveraged as a PET biomarker in neuroinflammation,[15-17] its elevated expression has also been reported in many types of cancer.[18] This overexpression in tumors has been reported to correlate with disease progression and diminished survival and can be indicative of aggressive and potentially metastatic tumors.[18] Within this context, our laboratory has investigated the use of TSPO PET ligands to image colon cancer,[8] breast cancer,[9] and glioma,[12,13,19] as these agents could potentially serve as useful cancer imaging biomarkers. Moreover, on a mechanistic level, we have utilized TSPO molecular imaging probes to visualize colon cancers arising in genetically engineered mice with aberrant *Tgf*βsignaling,[8] as well as tumors arising in mice following loss of *Apc* function.[20] These studies suggest the potential importance TSPO PET agents to detect key molecular events in oncology and to possibly serve as companion diagnostics alongside targeted inhibitors of these pathways.

We recently reported the first utilizations of two TSPO-specific PET ligands for quantitative assessment of TSPO expression in preclinical glioma, the aryloxyanilide *N*-[^{18}F]fluoroacetyl-*N*-(2,5-dimethoxybenzyl)-2-phenoxyaniline ([^{18}F]PBR06, [^{18}F]-**1**),[11] and the pyrazolopyrimidine *N*,*N*-diethyl-2-(2-(4-(2-[^{18}F]fluoroethoxy)phenyl)-5,7-dimethylpyrazolo[1,5-*a*]pyrimidin-3-yl)acetamide ([^{18}F]DPA-714, [^{18}F]-**2a**)[12] (**Figure 1**). Through focused library synthesis and structure−activity relationship (SAR) development of the 5,6,7-substituted pyrazolopyrimidine scaffold of [^{18}F]-**2a**, we developed 2-(5,7-

diethyl-2-(4-(2-[^{18}F]fluoroethoxy)phenyl)pyrazolo[1,5-*a*]pyrimidin-3-yl)-*N*,*N*–diethylacetamide ([^{18}F]-**2b**, [^{18}F]VUIIS1008), a novel and highly potent TSPO PET ligand exhibiting a 36-fold enhancement in affinity compared to [^{18}F]-**2a** and accessible in high radiochemical yield and specific activity.[13] Subsequent *in vivo* studies of [^{18}F]-**2b** demonstrated this agent to possess several properties for molecular imaging of TSPO-expressing cancers.[13,21]

In addition to the aryloxyanilides and pyrazolopyrimidines, pyridazinoindoles are another series of potent TSPO ligands, as represented by 7-chloro-*N*,*N*,5-trimethyl-4-oxo-3-phenyl-3,5-dihydro-4*H*-pyridazino[4,5-*b*]indole-1-acetamide (SSR180575, **3**).[22,23] Developed originally by Sanofi-Aventis, the specificity and high-affinity of **3** for TSPO has prompted research in cardiovascular[24,25] and renal pathologies,[26] as well as neurodegenerative indications,[23] inflammatory disorders,[22,27-29] and HIV pathogenesis.[30]

The goal of this study was to determine whether optimization of **3**, specifically at the N3 position, would yield TSPO ligands with comparable affinity and potential to serve as PET imaging ligands. These experiments led to the synthesis of **3** in only four steps and the subsequent development of 7-chloro-*N*,*N*,5-trimethyl-4-oxo-3(6-fluoropyridin-2-yl)-3,5-dihydro-4*H*-pyridazino[4,5-*b*]indole-1-acetamide (**14**), a novel pyridazinoindole TSPO ligand exhibiting binding comparable to **3** and structural features suitable for radiolabeling with fluorine-18 (^{18}F). Radiofluorination of either the 2-chloro (**15**) or 2-bromo (**16**) precursor gave 7-chloro-*N*,*N*,5-trimethyl-4-oxo-3(6-[^{18}F]fluoropyridin-2-yl)-3,5-dihydro-4*H*-pyridazino[4,5-*b*]indole-1-acetamide ([^{18}F]-**14**), which was subsequently evaluated *in vivo* in a preclinical model of glioma (C6). [^{18}F]-**14** exhibited modest accumulation in normal brain, yet robust accumulation in tumor tissue, which facilitated excellent imaging contrast. [^{18}F]-**14** was fully displaceable by administration of non-radioactive **14** halfway through the PET scan. Overall, these studies illuminate [^{18}F]-**14** as a promising, novel PET ligand for evaluating TSPO expression in gliomas and potentially other solid tumors and diseases.

The original synthesis of SSR180575 (**3**) remains a patented process at seven total steps.[31] Moreover, the patented SAR studies of **3** targeted four areas on the scaffold, the acetamide functionality at C1 and the N3, N5, and C7 positions of the tricyclic pyridazinoindole ring (**Figure 1**).[31,32] The synthesis developed and reported herein requires only four steps from a commercially available starting material (**Scheme 1**). A small library of pyridazinoindoles (**Table 1**) was assembled, with the point of divergence at the final condensation step with strategic arylhydrazines (**8**) (**Scheme 1**). The design of the library focused primarily on incorporation of fluorine onto an aromatic ring and potential substituents that would facilitate radiolabeling with ^{18}F.

The overall synthetic methodology is presented in **Scheme 1**. Starting from a commercially available indole (**4**), deprotonation with sodium hydride in DMF, followed by treatment with methyl iodide, gave the desired *N*-methylated intermediate (**5**) (85%). Acylation of (**5**) at C3 was achieved using $TiCl_4$ and methyl chloro-3-oxopropanoate in dichloroethane at 40 °C for 15 h, which gave keto diester **6** (46%). The necessary *N*,*N*-dimethylamide moiety at C1 (**7**) was achieved through displacement of the methoxy group of (**6**) with dimethylamine in

toluene and THF in a sealed tube at 110 °C for 15 h. Final condensation with phenylhydrazine (**8**, R=phenyl) gave the lead compound, SSR1805875 (**3**), in 32% yield. To date, this stands as the shortest reported synthesis of this particular TSPO ligand.

Diversification at the N3 position of **3** was achieved through condensation of key intermediate **7** with a series of monosubstituted aryl hydrazines (**8**) (31-50%). The hydrazines chosen focused upon variation of the endogenous N3-phenyl ring, with particular attention towards preliminary SAR and functional groups amenable to PET ligand development, namely the presence of a fluorine atom and groups that would facilitate radiolabeling with ^{18}F through an ipso-type substitution. The groups explored included: a substituted phenyl ring (2-, 3-, 4-positions) (**9**-**12**); a 2-pyridyl ring (**13**); a substituted 2-pyridyl ring (**14**-**16**).

To evaluate binding to TSPO, radiometric binding assays were carried out with the compounds in a variety of athymic nude rat cell lysates (C6, heart, kidney) using *N*-(*sec*-butyl)-1-(2-chlorophenyl)-*N*-methyl-[^{3}H]-isoquinoline-3-carboxamide ([^{3}H]PK11195).[11,12] For central benzodiazepine receptor (CBR) binding, radioligand displacement was carried out against [^{3}H]flunitrazepam in healthy, athymic nude rat brain lysate. Affinities are expressed as K_i ± S.E.M. (pM) in **Table 1**. All experiments were performed in triplicate.

Of the eight analogs synthesized, seven proved extremely potent in all three lysates, with K_i values comparable to those of the parent SSR180575 (**3**): in C6 lysate, 0.280-2.34 pM *versus* 1.23 pM for **3**; in heart 0.180-3.21 pM *versus* 0.762 pM for **3**; in kidney, 0.212-2.21 pM *versus* 0.596 pM for **3**. Only one analog, compound **13**, bearing a 2-pyridyl ring at N3, did not appreciably bind TSPO in any of the lysates. Interestingly, a portion of the compounds synthesized showed evidence of mixed (low, high) binding affinities. In C6 lysate, compounds **12** and **14** demonstrated high-affinity binding at 0.671 and 1.19 pM, and low-affinity binding at 1770 and 3020 pM, respectively. Compound **12** demonstrated similar mixed binding in kidney lysate (0.459 and 969 pM), but not the heart. While multiple PK11195 TSPO binding sites have been reported and merit consideration,[33] recent research has also implicated a genetic polymorphism for such binding variations in the human brain.[34,35] However, genetic sequencing of the C6 cell line from the specific clonal population used for this study confirmed its wild-type status. The mixed binding we observed could potentially be a result of overlapping points of interaction that the analogs and PK11195 possess for TSPO.

Overall, the modifications made to lead compound **3**, with the exception of **13**, were well tolerated. While substitution of the N3-phenyl ring with 2-pyridine did adversely affect binding across all three lysates, comparable biological activity was regained with halogen substitution at the 3-position of the ring (**14**-**16**). This influence on potency could be attributed to an electronic effect of the halogen atom and merits further consideration in future studies. Similarly, 2-, 3-, and 4-fluorosubstitution on the endogenous phenyl ring with fluorine (**9**, **10**, **12**, respectively) proved to minimally affect TSPO affinity, as did 4-nitro-substitution (**11**). This series of compounds are among the most potent ligands reported for TSPO in C6 glioma (**1** K_i = 6170 pM;[11] **2a** K_i = 9730 pM;[12] **2b** K_i = 270 pM[13]). Moreover, in our lab, compound **14** represents a 1000-fold increase in potency over **2b**.

Of the synthesized series, the 3-fluoro analog **10** was initially considered the candidate PET tracer, particularly given its activity and ready availability of its 3-nitro precursor (**11**). However, effective substitution of a nitro group with $^{18}F^-$ on a benzene ring requires a highly deactivated ring system, preferably with electron-withdrawing groups either *ortho* or *para* to the nitro moiety. Neither was the case for **11** as a precursor. Similar arguments could also be made for consideration of **9** or **12** as PET tracer candidates. Compound **14** was ultimately chosen as the candidate PET tracer, with **15** and **16** as possible precursors. The selectivity of **14** for TSPO over CBR was evaluated through displacement of [^{3}H]flunitrazepam in rat cerebral cortex membranes (**Table 1**). The selectivity of **14** for TSPO over CBR was verified with [^{3}H]flunitrazepam, which gave a K_i >10 μM.

Isotopic labeling of **3** with both ^{11}C and ^{18}F has been previously reported in the patent literature.[36] In the research literature, Thominiaux *et al.* reported ^{11}C labeling at the 5-methylpyridazino[4,5-*b*]indole ([*indole-N-methyl*-^{11}C]SSR180575) and *N*,*N*-dimethylacetamide ([*acetamide-N-methyl*-^{11}C]SSR180575)[37] moieties. Within the context of radiochemical yield and purity, and *in vivo* pharmacological properties, [*indole-N-methyl*-^{11}C]SSR180575 was advanced as a candidate for imaging neuroinflammation[37] and afforded higher image contrast when compared to the traditional isoquinoline [^{11}C]PK11195 in a model of acute neuroinflammation (rat).[38] Moreover, competition studies demonstrated a high specific binding of [^{11}C]SSR180575 for TSPO.[38] However, as far as the authors are aware, no studies to date have been reported for the use of isotopically labeled SSR180575 for PET imaging in oncology. Since our goal was to explore **3** as a potential radiopharmaceutical lead for translation into preclinical cancer imaging studies, radiofluorination was deemed to be the most effective means to achieve this goal. Though useful in the research setting, the 20.4 min half-life of ^{11}C limits broader utility of the tracer (shipment to satellite locations, dynamic PET studies), thus making ^{18}F (109.4 min half-life) an attractive alternative.

We initially applied microfluidic-radiolabeling approaches to elucidate stability and ascertain labeling feasibility of precursors **15** and **16**. Using a commercial microfluidic module (NanoTek®) that enabled carefully controlled stoichiometry between [^{18}F]$^-$ and precursor at set temperatures (°C) with controllable reaction times (μL/min flow rates), we carried out multiple, small-scale, sequential radiolabelings in a relatively short amount of time, allowing rapid optimization of labeling conditions (**Table 2**). The information gathered with the NanoTek® module was used to better inform the transition to the GE TRACERlab™ $FX_{F\text{-}N}$ module for larger, preclinical-scale productions. Using cyclotron-generated $^{18}F^-$ and K^+-$K^{2.2.2}/K_2CO_3$ in anhydrous DMSO, a series of reaction temperatures (80-180 °C) at a transfer rate of 40 μL/min was investigated, with product formation monitored by radio-TLC for % ^{18}F-incorporation (**Table 2**). For the chloro precursor (**15**), product formation was observed at 180 °C (1.41%) at a transfer rate of 40 μL/min. Maintaining a reaction temperature of 180 °C and decreasing the transfer rate to 14 μL/min gave modest incorporation (5.2%, **Table 2**, *entry 3*). Similar results were obtained using precursor **16** (**Table 2**, *entry 6*). Despite modest yields, the data generated from these experiments also highlighted the thermal stability (up to 180 °C) of both **15** and **16**, verified by HPLC of crude reaction mixtures. Bromo-precursor **16** was ultimately chosen going

forward given its optimal chromatographic resolution from the final product ([^{18}F]-**14**). These observations provided a confident basis to pursue the radiolabeling reaction in a sealed system at 180 °C for a longer period of time.

Adaptation of these reaction conditions to large-scale box productions enabled preclinical production of [^{18}F]-**14** in the GE TRACERlab™ FX_{F-N} module with labeling conditions of 170 °C for 15 min. A lowering of the reaction temperature from 180 to 170 °C was deemed necessary due to the limitations of heating reliability at such an extreme temperature using the TRACERlab™ platform. Purification of [^{18}F]-**14** was carried out with preparative HPLC in 45% ethanol and 55% water. The retention time of [^{18}F]-**14** was 23-28 min according to gamma detection and corresponded to the UV retention time of nonradioactive **14**. Radiochemical purity was consistently greater than 99% (n=9), with decay-corrected yields ranging from 9.3-19.3% and specific activities as high as 5559 Ci/mmol (206 TBq/mmol) (n=9). However, the apparent specific activity was diminished using 42.5% ethanol and 57.5% water, despite the longer retention time.

The *in vivo* performance of [^{18}F]-**14** was evaluated in glioma-bearing (C6), male Wistar rats using microPET imaging, with a typical study shown in **Figure 2**. MRI (T_2-weighted) was used to localize tumors and for registration of anatomical features with PET (**Fig. 2A**).[11,12,18] Dynamic PET imaging with [^{18}F]-**14** illustrated that the majority of tracer accumulation in the brain was localized to the tumor, with modest accumulation that exceeded plasma in contralateral, non-tumor brain (**Fig. 2B** & **2C**). The tumor-selective characteristics of [^{18}F]-**14** afforded excellent imaging contrast between tumor and contralateral tissue. **Figure 2G** illustrates time−activity curves (TACs) typical of representative studies for tumor (blue), normal brain (green), and plasma (red) over a 90-min dynamic acquisition. After an initial spike in radioactivity consistent with tracer injection and rapid distribution, [^{18}F]-**14** quickly cleared the plasma (red). We found that [^{18}F]-**14** accumulation in the tumor (blue), relative to normal brain (green), reached a tumor-to-normal brain ratio greater than 10:1. Preliminary radio-TLC analysis of plasma samples (2, 12, 30, 60 min) taken during the scan (n=2) suggested minimal tracer metabolism over the 60 minutes (% parent at 60 min > 90%).

To validate the PET, imaging-matched brains were processed for *post-mortem* staining and immunohistochemistry for TSPO. *Ex vivo* histological analysis correlated well with PET imaging data, with close agreement between tumor tissue (H&E, **Fig. 2E**), elevated TSPO expression (immunohistochemistry, **Fig. 2F**), and tumor accumulation of [^{18}F]-**14** (**Fig. 2D**).

To evaluate the *in vivo* TSPO specificity of [^{18}F]-**14**, we performed displacement studies in C6-bearing rats using the non-radioactive analog (**14**). As shown in the TAC in **Figure 2H**, during the dynamic PET study, a bolus (IV) infusion of nonradioactive **14** (10 mg/kg) was administered approximately 30 minutes after injection of [^{18}F]-**14**. Summation of the first 30 minutes of the PET scan prior to injection of cold **14** (0–30 min) demonstrated typical accumulation characteristics of [^{18}F]-**14**. However, summation of the final 30 minutes of the PET scan (30– 60 min) demonstrated significant displacement of [^{18}F]-**14** from tumor tissue (blue). TAC analysis demonstrated that after injection of **14**, tumor binding was reduced to approximately 40% of the peak tumor uptake. During tumor displacement, we observed a

minor influx of tracer into normal brain (green). The displaced [^{18}F]-**14** then rapidly cleared the normal brain and entered the plasma, subsequently elevating plasma (red) radioactivity. These studies suggest a level of displaceable binding indicative of a high degree of specific binding and reversibility of [^{18}F]-**14** to TSPO in tumor tissue.

In this work, we report the shortest published synthesis of the pyridazinoindole TSPO ligand SSR180575 (**3**) to date. Initial SAR exploration at the N3 position of **3** provided a series of analogs of comparable potency, one of which (**14**) could be adapted into a potential PET imaging tracer ([^{18}F]-**14**). Subsequent preclinical studies illuminated [^{18}F]-**14** as a promising, novel TSPO PET ligand for imaging glioma. Compared to previous TSPO PET ligands in oncology, the first generation ligand [^{11}C]PK11195[39] and the second generation ligands [^{18}F]PBR06,[19] [^{18}F]DPA-714,[12] and [^{18}F]VUIIS1008,[13,21] [^{18}F]-**14** has demonstrated improved binding affinity and *in vivo* imaging characteristics. These advantages, in addition to the *in vivo* stability and high signal-to-noise achieved between tumor and surrounding normal brain, suggest the potential of this PET ligand for detection of TSPO-expressing tumors in the brain and neuroinflammation. Future head-to-head comparisons between this tracer and emerging, potent TSPO ligands[13,21] are underway, as well as exploration of other promising applications in oncology, neuroinflammation, and other diseases.

Supplementary Material

Refer to Web version on PubMed Central for supplementary material.

Acknowledgments

We acknowledge funding from the National Institutes of Health (K25 CA127349, P50 CA128323, S10 RR17858, U24 CA126588, 1R01 CA163806, P50 CA095103, P30 DK058404), The Kleberg Foundation, and The Lustgarten Foundation. Dr. M. Noor Tantawy, George H. Wilson, and Dr. Daniel Colvin are acknowledged for support of the imaging studies.

References

1. Dhermain FG, Hau P, Lanfermann H, Jacobs AH, van den Bent MJ. Lancet Neurol. 2010; 9:906. [PubMed: 20705518]
2. Rheims S, Rubi S, Bouvard S, Bernard E, Streichenberger N, Guenot M, Le Bars D, Hammers A, Ryvlin P. Neurooncology. 2014
3. Jansen NL, Suchorska B, Wenter V, Eigenbrod S, Schmid-Tannwald C, Zwergal A, Niyazi M, Drexler M, Bartenstein P, Schnell O, Tonn JC, Thon N, Kreth FW, la Fougere C. Journal of nuclear medicine : official publication, Society of Nuclear Medicine. 2014; 55:198.
4. Schwarzenberg J, Czernin J, Cloughesy TF, Ellingson BM, Pope WB, Grogan T, Elashoff D, Geist C, Silverman DH, Phelps ME, Chen W. Clinical cancer research : an official journal of the American Association for Cancer Research. 2014; 20:3550. [PubMed: 24687922]
5. Goldman S, Pirotte BJ. Methods Mol Biol. 2011; 727:291. [PubMed: 21331940]
6. la Fougere C, Suchorska B, Bartenstein P, Kreth FW, Tonn JC. Neuro Oncol. 2011; 13:806. [PubMed: 21757446]
7. Pirotte B, Goldman S, Massager N, David P, Wikler D, Vandesteene A, Salmon I, Brotchi J, Levivier M. Journal of nuclear medicine : official publication, Society of Nuclear Medicine. 2004; 45:1293.

8. Deane NG, Manning HC, Foutch AC, Washington MK, Aronow BJ, Bornhop DJ, Coffey RJ. Mol Cancer Res. 2007; 5:341. [PubMed: 17426249]
9. Wyatt SK, Manning HC, Bai M, Bailey SN, Gallant P, Ma G, McIntosh L, Bornhop DJ. Mol Imaging Biol. 2010; 12:349. [PubMed: 19949989]
10. Manning HC, Goebel T, Thompson RC, Price RR, Lee H, Bornhop DJ. Bioconjug Chem. 2004; 15:1488. [PubMed: 15546219]
11. Buck JR, McKinley ET, Hight MR, Fu A, Tang D, Smith RA, Tantawy MN, Peterson TE, Colvin D, Ansari MS, Baldwin RM, Zhao P, Guleryuz S, Manning HC. Journal of nuclear medicine : official publication, Society of Nuclear Medicine. 2011; 52:107.
12. Tang D, Hight MR, McKinley ET, Fu A, Buck JR, Smith RA, Tantawy MN, Peterson TE, Colvin DC, Ansari MS, Nickels M, Manning HC. Journal of nuclear medicine : official publication, Society of Nuclear Medicine. 2012; 53:287.
13. Tang D, McKinley ET, Hight MR, Uddin MI, Harp JM, Fu A, Nickels ML, Buck JR, Manning HC. Journal of medicinal chemistry. 2013; 56:3429. [PubMed: 23521048]
14. Papadopoulos V, Baraldi M, Guilarte TR, Knudsen TB, Lacapere JJ, Lindemann P, Norenberg MD, Nutt D, Weizman A, Zhang MR, Gavish M. Trends Pharmacol Sci. 2006; 27:402. [PubMed: 16822554]
15. Varrone A, Mattsson P, Forsberg A, Takano A, Nag S, Gulyas B, Borg J, Boellaard R, Al-Tawil N, Eriksdotter M, Zimmermann T, Schultze-Mosgau M, Thiele A, Hoffmann A, Lammertsma AA, Halldin C. Eur J Nucl Med Mol Imaging. 2013; 40:921. [PubMed: 23436070]
16. Suridjan I, Rusjan PM, Voineskos AN, Selvanathan T, Setiawan E, Strafella AP, Wilson AA, Meyer JH, Houle S, Mizrahi R. Neuroimage. 2013
17. Takano A, Piehl F, Hillert J, Varrone A, Nag S, Gulyas B, Stenkrona P, Villemagne VL, Rowe CC, Macdonell R, Tawil NA, Kucinski T, Zimmermann T, Schultze-Mosgau M, Thiele A, Hoffmann A, Halldin C. EJNMMI research. 2013; 3:30. [PubMed: 23618062]
18. Batarseh A, Papadopoulos V. Mol Cell Endocrinol. 2010
19. Buck JR, Saleh S, Uddin MI, Manning HC. Tetrahedron letters. 2012; 53:4161. [PubMed: 23180892]
20. Powell AE, Vlacich G, Zhao ZY, McKinley ET, Washington MK, Manning HC, Coffey RJ. American journal of physiology. Gastrointestinal and liver physiology. 2014; 307:G16. [PubMed: 24833705]
21. Tang D, Nickels ML, Tantawy MN, Buck JR, Manning HC. Mol Imaging Biol. 2014
22. Bribes E, Bourrie B, Esclangon M, Galiegue S, Vidal H, Casellas P. Eur J Pharmacol. 2002; 452:111. [PubMed: 12323392]
23. Ferzaz B, Brault E, Bourliaud G, Robert JP, Poughon G, Claustre Y, Marguet F, Liere P, Schumacher M, Nowicki JP, Fournier J, Marabout B, Sevrin M, George P, Soubrie P, Benavides J, Scatton B. J Pharmacol Exp Ther. 2002; 301:1067. [PubMed: 12023539]
24. Leducq N, Bono F, Sulpice T, Vin V, Janiak P, Fur GL, O'Connor SE, Herbert JM. J Pharmacol Exp Ther. 2003; 306:828. [PubMed: 12928523]
25. Vin V, Leducq N, Bono F, Herbert JM. Biochemical and biophysical research communications. 2003; 310:785. [PubMed: 14550272]
26. Kunduzova OR, Escourrou G, De La Farge F, Salvayre R, Seguelas MH, Leducq N, Bono F, Herbert JM, Parini A. Journal of the American Society of Nephrology : JASN. 2004; 15:2152. [PubMed: 15284300]
27. Galiegue S, Tinel N, Casellas P. Curr Med Chem. 2003; 10:1563. [PubMed: 12871127]
28. Bribes E, Galiegue S, Bourrie B, Casellas P. Immunology Letters. 2003; 85:13. [PubMed: 12505191]
29. Bribes E, Bourrie B, Casellas P. Immunology Letters. 2003; 88:241. [PubMed: 12941483]
30. Leducq-Alet N, Vin V, Savi P, Bono F. Biochemical and biophysical research communications. 2010; 399:475. [PubMed: 20621066]
31. Ferzaz B, Benavides J, Marguet F, Froissant J, Marabout B, Evanno Y, Sevrin M, Janiak P, Organization WIP. Sanofi-Synthelabo: France. 2000:32.

32. Evanno Y, Dubois L, Sevrin M, Marguet F, Froissant J, Bartsch R, Gille C, Organization WIP. Synthelabo S. A.: France. 1999
33. Scarf AM, Kassiou M. Journal of nuclear medicine : official publication, Society of Nuclear Medicine. 2011; 52:677.
34. Owen DR, Yeo AJ, Gunn RN, Song K, Wadsworth G, Lewis A, Rhodes C, Pulford DJ, Bennacef I, Parker CA, StJean PL, Cardon LR, Mooser VE, Matthews PM, Rabiner EA, Rubio JP. Journal of cerebral blood flow and metabolism : official journal of the International Society of Cerebral Blood Flow and Metabolism. 2012; 32:1.
35. Yoder KK, Nho K, Risacher SL, Kim S, Shen L, Saykin AJ. Journal of nuclear medicine : official publication, Society of Nuclear Medicine. 2013; 54:1320.
36. Benavides, J.; Boutin, H.; Castel, M-N.; Damont, A.; Dolle, F.; Hantraye, P.; Marguet, F.; Rooney, T.; Rivron, L.; Tavitian, B.; Thominiaux, C.; Sanofi-Aventis, Fr. Commissariat a l'Energie Atomique C.E.A.; France: 2010. p. 40
37. Thominiaux C, Damont A, Kuhnast B, Demphel S, Helleix SL, Boisnard S, Rivron L, Chauveau F, Boutin H, Camp NV, Boisgard R, Roy S, Allen J, Rooney T, Benavides J, Hantraye P, Tavitian B, Dolle F. Journal of Labelled Compounds & Radiopharmaceuticals. 2010; 53:767.
38. Chauveau F, Boutin H, Van Camp N, Thominiaux C, Hantraye P, Rivron L, Marguet F, Castel MN, Rooney T, Benavides J, Dolle F, Tavitian B. Eur J Nucl Med Mol Imaging. 2011; 38:509. [PubMed: 20936410]
39. Starostarubinstein S, Ciliax BJ, Penney JB, Mckeever P, Young AB. Proceedings of the National Academy of Sciences of the United States of America. 1987; 84:891. [PubMed: 3027710]

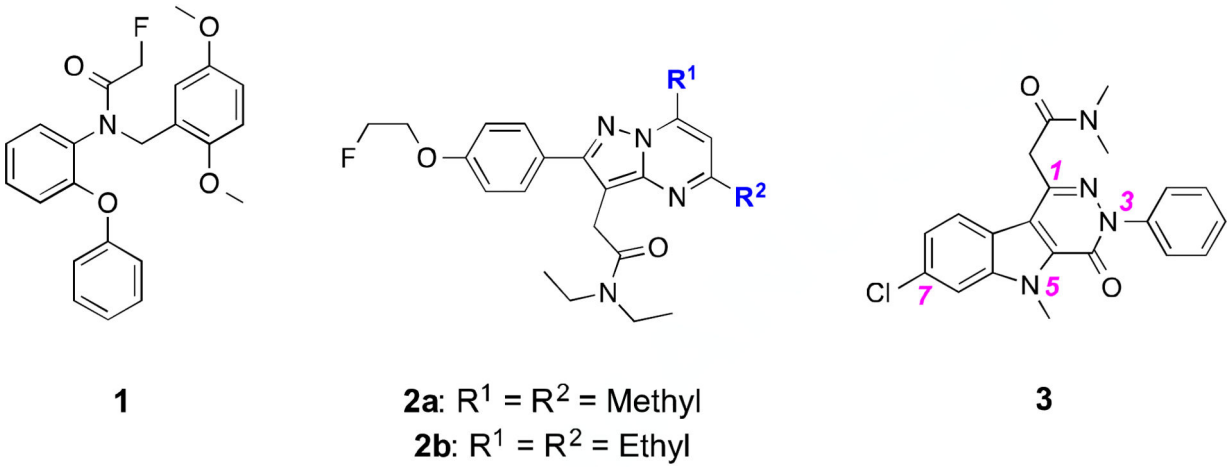

1 **2a**: $R^1 = R^2$ = Methyl **3**

2b: $R^1 = R^2$ = Ethyl

Figure 1.

Representative TSPO ligand scaffolds: Aryloxyanilide (**1**, PBR06); Pyrazolopyrimidine (**2a**, DPA-714; **2b**, VUIIS1008); Pyridazinoindole (**3**, SSR180575).

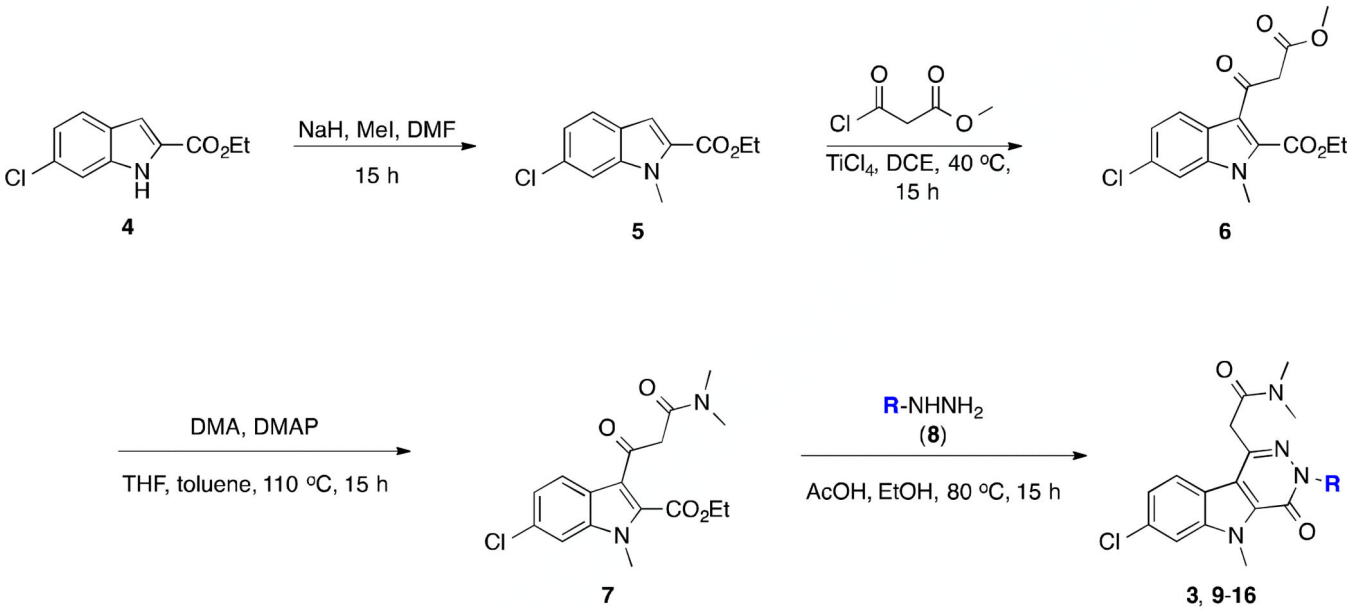

Scheme 1.

Synthetic methodology developed to generate SSR180575 (**3**) and a focused library of N3-substituted pyridazinoindoles (**9**-**16**).

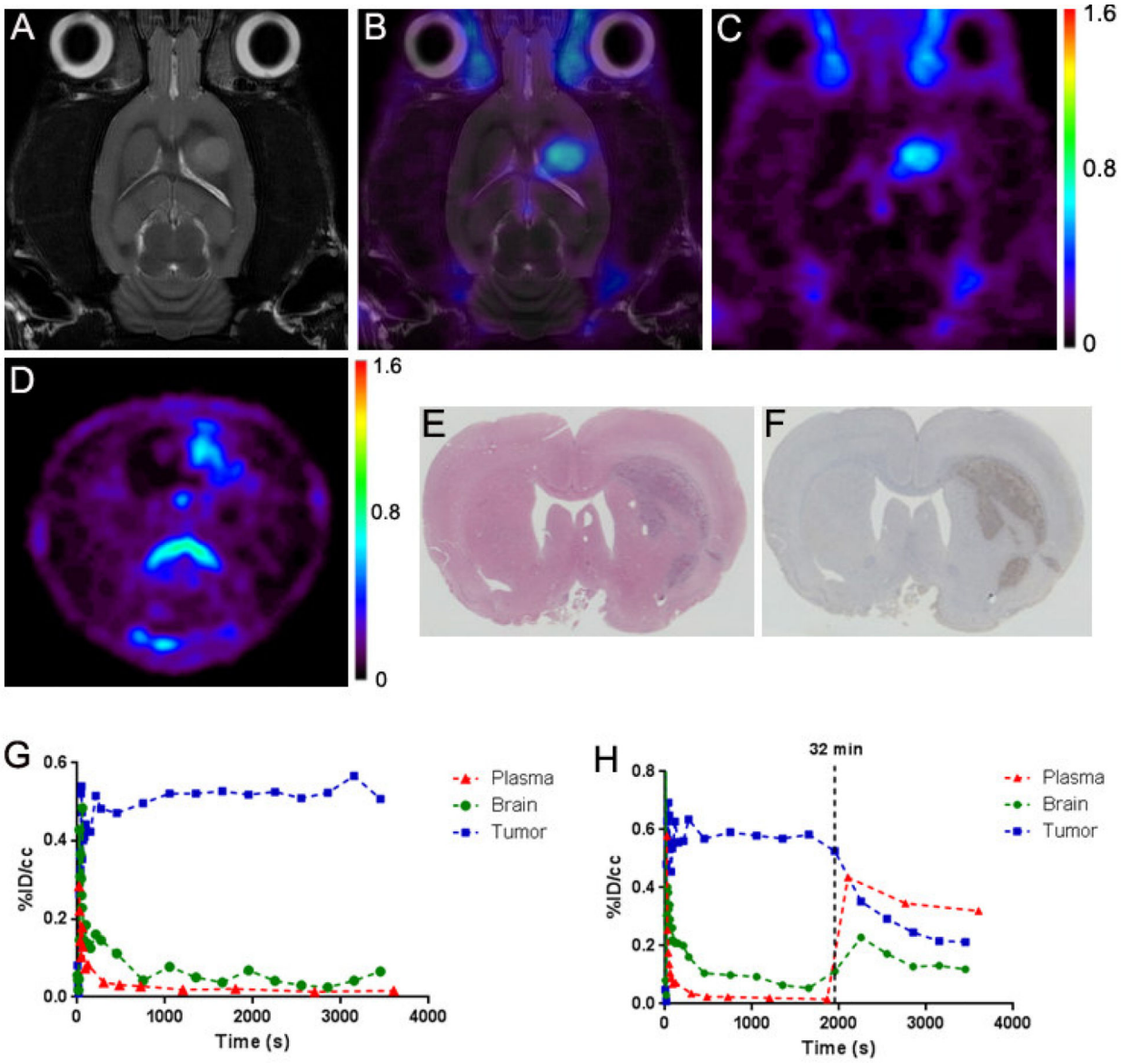

Figure 2.

Imaging of preclinical glioma using [^{18}F]-**14**. (A) T_2–weighted MRI (*coronal*). (B) Fused MRI-PET (*coronal*). (C) Dynamic PET (*coronal*). (D) Dynamic PET (*axial*). (E) H&E histology. (F) TSPO immunohistochemistry. (G) Typical dynamic PET TAC. (H) Displacement study PET TAC.

Table 1

Affinity of Pyridazinoindoles

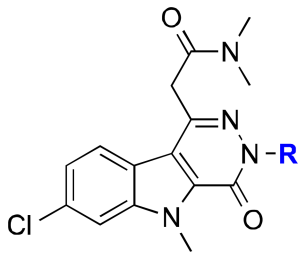

Compd	R	C6 Glioma Ki (pM)[b]	Heart Ki (pM)[b]	Kidney Ki (pM)[b]
3[a]	Ph	1.23 ± 0.08	0.762 ± 0.15	0.596 ± 0.04
9	2-fluorophenyl	0.422 ± 0.06	0.591 ± 0.10	1.18 ± 0.04
10	3-fluorophenyl	0.280 ± 0.07	0.180 ± 0.02	0.212 ± 0.02
11	3-nitrophenyl	0.889 ± 0.2	1.18 ± 0.09	0.678 ± 0.2
12	4-fluorophenyl	0.671 ± 0.2; 3020 ± 1007[d]	0.877 ± 0.03	0.459 ± 0.03; 969 ± 752[d]
13	2-pyridyl	2409 ± 795.4	4936 ± 662.3	6796 ± 830.9
14[c]	3-fluoro-2-pyridyl	|1.19 ± 0.05; 1770 ± 232.6[d]	3.21 ± 0.4	2.21 ± 0.4
15	3-chloro-2-pyridyl	2.34 ± 0.4	0.676 ± 0.08	0.495 ± 0.03
16	3-bromo-2-pyridyl	1.48 ± 0.2	0.281 ± 0.01	0.965 ± 0.02

[a] SSR180575.

[b] Ki ± S.E.M. *versus* [^{3}H]PK11195.

[c] Ki *versus* [^{3}H]flunitrazepam in rat brain lysate >10 μM.

[d] Mixed affinity binding. All lysates procured from athymic nude rats. All experiments performed in triplicate.

Table 2

Initial radiofluorination of precursor **15 & 16** using microfluidics.

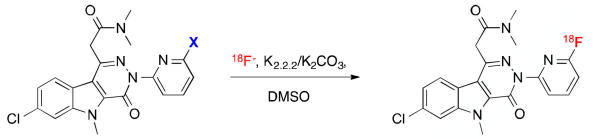

15/16* **[^{18}F]-14**

Run	X	Temp (°C)	Transfer Rate (μl)	RCY (%)
1	Cl	140	40	0
2	Cl	160	40	0
3	Cl	180	14	5.2
4	Br	140	40	0
5	Br	160	40	1
6	Br	180	60	7

*Precursors **15 & 16** stable up to 180 °C.